

Universität des Saarlandes



Fachbereich 9 – Mathematik

Mathematischer Preprint

**Mathematical concepts of open quantum
boundary conditions**

Anton Arnold

Preprint No. 11

Saarbrücken 2000

Universität des Saarlandes



Fachbereich 9 – Mathematik

**Mathematical concepts of open quantum
boundary conditions**

Anton Arnold

Fachbereich Mathematik
Universität des Saarlandes
D-66123 Saarbrücken
Germany
arnold@num.uni-sb.de

submitted: March 28, 2000

Preprint No. 11

Saarbrücken 2000

Edited by
FB 9 – Mathematik
Im Stadtwald
D-66041 Saarbrücken
Germany

Fax: + 49 681 302 4443
e-mail: preprint@math.uni-sb.de
WWW: <http://www.math.uni-sb.de/>

Abstract

This paper is concerned with the derivation and the numerical discretization of open boundary conditions for the 1D Schrödinger equation in order to simulate quantum devices. New discrete transparent boundary conditions are presented that are able to handle the situation of a continuous plane wave influx into a device. Also, we give a review of various formulations of boundary conditions that are used within the Schrödinger and the Wigner formalism of quantum mechanics, and we discuss their mathematical properties.

1 Introduction

The electrical properties of many semiconductor devices of today's nano-scale technology (resonant tunneling diodes and quantum waveguides, e.g.) crucially depend on quantum mechanical effects. Thus, one often has to use fully quantum mechanical models when describing the carrier (electron) transport within such devices. Due to the intrinsic non-locality of quantum mechanics it is far from trivial to impose physically correct boundary conditions (BCs) that are also numerically tractable.

At the insulating portions of the device boundaries it is physically sensible to impose homogeneous Dirichlet BCs for the Schrödinger wave function, e.g. At device contacts, however, *open boundary conditions* have to be employed. In recent years lots of progress towards the understanding of such open BCs has been made. In this paper we will give an overview of recent mathematical results on open BCs for both the Schrödinger and the Wigner formulations of quantum mechanics. We shall discuss modeling questions and present various analytical and numerical results for stationary and transient problems. Our main focus will be new numerical results on transparent boundary conditions for the Schrödinger equation that are used to simulate quantum waveguides.

For developing novel semiconductor devices it is already standard today to employ sophisticated simulation tools during the designing process. There, engineers are interesting both in stationary simulation results ($I - V$ curves, conductance, possible bistabilities, e.g.) and in the transient behavior of the device (switching times, oscillation frequencies, e.g.). For an account on the vast literature on this field we refer to [9], [10], [13], [20], [25], and references therein.

For the simulation quality of quantum devices (quantum waveguides and resonant tunneling diodes, e.g.) a careful modeling and numerical discretization of the BCs are of paramount importance. Throughout this article we shall assume that a quantum mechanical semiconductor model (Schrödinger or Wigner equation) is given on a large (possibly unbounded) domain. For practical purposes (numerical effort, e.g.) we then assume that the actual modeling and simulation are confined to a finite subregion: for the examples we have in mind this might be the active region of a quantum waveguide or the channel of a resonant-tunneling-FET. At the boundary of this subregion one then introduces an *artificial boundary condition*, assuming that the incoming flux of charge carriers is known. The "outside region" hence acts like a

quantum mechanical reservoir that is connected to the considered device by leads. While these boundaries sometimes coincide with physical interfaces, we shall not discuss here the physics of quantum contacts beyond the coupling to an exterior reservoir. Currently, several research groups are investigating the possibility to couple classical and quantum mechanical models. For such a quantum/classical coupling for a stationary kinetic model we refer to [7].

Now we briefly introduce the two evolution models that will be considered in this paper. Numerical simulations of quantum waveguides and resonant tunneling structures are typically based on the 1D or 2D Schrödinger equation ([9]) or on the Wigner equation (so far only in 1D): [12], [15], [17], [27]. For a recent review of numerical methods for quantum transport problems we refer to [25].

The transient Schrödinger equation for the electron wave function $\psi(x, t)$ reads

$$i\hbar\psi_t = -\frac{\hbar^2}{2m^*}\Delta_x\psi + V(x, t)\psi, \quad x \in \Omega, \quad (1.1)$$

where V denotes the (possibly time-dependent) potential energy of the electron, m^* its effective mass, and \hbar is the Planck constant.

The kinetic Wigner equation governs the time evolution of the Wigner function $w(x, v, t)$:

$$w_t + v \cdot \nabla_x w - \frac{1}{m^*}\Theta[V]w = 0, \quad x \in (0, L), \quad v \in \mathbb{R}, \quad (1.2)$$

with the pseudo-differential operator

$$\begin{aligned} \Theta[V]w &= i\partial V\left(x, \frac{\nabla_v}{i}, t\right)w \\ &= \frac{i}{2\pi} \int_{\mathbb{R}_\eta} \int_{\mathbb{R}_{v'}} \partial V(x, \eta, t)w(x, v', t)e^{i(v-v')\cdot\eta} dv' d\eta, \\ \partial V(x, \eta, t) &= \frac{m^*}{\hbar} \left(V\left(x + \frac{\hbar\eta}{2m^*}, t\right) - V\left(x - \frac{\hbar\eta}{2m^*}, t\right) \right). \end{aligned} \quad (1.3)$$

The (real valued) Wigner function resembles a kinetic phase-space distribution function. However, it may take both positive and negative values (cf. [20] for details). This phase-space formulation of quantum mechanics is essentially equivalent to the Schrödinger equation, but it allows for a simpler coupling of different pure quantum states by incorporating scattering terms on the RHS of (1.2). Due to the numerical complexity of (1.2) only 1D Wigner-simulations of quantum semiconductor devices have been carried out so far. So we shall also confine ourselves here to the 1D case.

Due to the small time and length scales of the considered quantum devices, the transport regime is mostly ballistic for such applications. Hence we shall not include scattering terms in our discussion of open BCs. But since they are typically local in x , they do not complicate the

situation very much, anyhow. For an analysis of *absorbing BCs* for the Wigner equation with a relaxation term we refer to [1].

This paper is organized as follows: in §2 we discuss transparent BCs for the stationary 1D Schrödinger equation from the analytical and numerical point of view. Numerical examples illustrate how they ‘work’. In §3 we investigate transparent BCs for the transient Schrödinger equation, in particular when a plane wave inflow into the computational domain is prescribed. Our main emphasis will be on their stable and accurate numerical discretization. With these BCs we then simulate the transient response of a quantum waveguide model when applying a bias. In §4 we review inflow BCs for the stationary Wigner equation and absorbing BCs for the transient situation.

2 Transparent BCs for the stationary Schrödinger equation

First we consider the stationary Schrödinger equation on the real line:

$$-\frac{\hbar^2}{2m^*}\psi_{xx} + V(x)\psi = E\psi, \quad x \in \mathbb{R}, \quad (2.1)$$

where E is the (constant-in- x) energy of a steady state. We assume that the “device region” (a resonating cavity of a quantum waveguide, e.g.) is represented by the spatial interval $(0, L)$ and it is connected to two leads on either side. For simplicity we shall assume here that the (real valued) potential $V(x)$ is given, and not self-consistently coupled to the wave function. But a Schrödinger–Poisson coupling within the device region would not change our discussion of the boundary conditions. Further, we assume that V is constant in the leads:

$$\begin{aligned} V(x) &= 0, & x \leq 0, \\ V(x) &= V_L, & x \geq L. \end{aligned}$$

Let the (stationary) scattering state $\psi(x)$ be the result of a plane wave entering the device region via the left lead:

$$\psi^{in}(x) = e^{ikx}, \quad x < 0, \quad (2.2)$$

with the wave vector $k > 0$ and the energy $E = \frac{k^2\hbar^2}{2m^*}$. This incoming wave gives rise to a reflected plane wave

$$\psi^r(x) = R_k e^{-ikx}, \quad x < 0 \quad (2.3)$$

and a transmitted wave

$$\psi^t(x) = T_k e^{i\sqrt{k^2 - 2m^*V_L/\hbar^2}x}, \quad x > L. \quad (2.4)$$

In the left lead the steady state solution hence takes the form

$$\psi(x) = \psi^{in}(x) + \psi^r(x), \quad x < 0. \quad (2.5)$$

The (complex valued) reflection and transmission coefficients satisfy $|R_k|^2 + |T_k|^2 = 1$ for any $k > 0$ and they are obtained by solving the Schrödinger equation (2.1).

After formulating the stationary whole space problem for $\psi(x)$, $x \in \mathbb{R}$ we now turn to the equivalent problem with *transparent boundary conditions* (TBC). The idea of TBCs is to reformulate the above problem on a finite spatial domain by introducing artificial BCs at (or outside of) the boundary of the device region. This should be done in a way such that the solutions of the two problems coincide on the bounded domain. Since the potential V is constant in the leads we shall place these artificial BCs at $x = 0$ and $x = L$. The TBCs can now be obtained by eliminating the a-priorily unknown coefficients R_k and T_k from (2.5) and (2.4), resp. For a fixed wave vector k of the incoming wave this yields the boundary value problem (BVP)

$$\begin{aligned} -\frac{\hbar^2}{2m^*}\varphi_{xx} + V(x)\varphi &= \frac{k^2\hbar^2}{2m^*}\varphi, & 0 < x < L, \\ \varphi'(0) + ik\varphi(0) &= 2ik, \\ \varphi'(L) &= i\sqrt{k^2 - 2m^*V_L/\hbar^2}\varphi(L). \end{aligned} \quad (2.6)$$

This BVP admits a unique solution $\varphi \in W^{2,\infty}(0, L)$ for any potential $V \in L^\infty(0, L)$ and any $k > 0$ (cf. [8]). As intended we have $\psi(x) = \varphi(x)$ on $(0, L)$. Such TBCs (in 2D) were introduced in [18] to numerically solve the stationary Schrödinger equation using a finite element method. Here we are interested in a finite difference discretization of (2.6) and particularly of the two TBCs. This will serve as a basis for our transient calculations in the next section.

For notational simplicity we shall set $\hbar = m^* = 1$ for the rest of this section. With the uniform grid points $x_j = j\Delta x$, $j = 0, \dots, J$ ($L = J\Delta x$) and the approximation $\varphi_j \sim \varphi(x_j)$ a simple scheme for the Schrödinger equation (2.1) reads

$$-\frac{1}{2} \frac{\varphi_{j-1} - 2\varphi_j + \varphi_{j+1}}{\Delta x^2} = (E - V_j)\varphi_j, \quad j = 1, \dots, J-1, \quad (2.7)$$

with $V_j = V(x_j)$.

First we consider the case $V = 0$ which, by assumption, holds in the left exterior region $x \leq 0$. There, (2.7) admits two *discrete plane wave solutions* of the form

$$\varphi_j = \alpha^j, \quad j \leq 0,$$

with

$$\alpha_{1,2} = 1 - E\Delta x^2 \pm i\sqrt{2E\Delta x^2 - E^2\Delta x^4}. \quad (2.8)$$

Under the assumption $\Delta x < \sqrt{\frac{2}{E}}$ we have $|\alpha| = 1$, as needed for a (discrete) plane wave. This assumption is no real restriction, but anyhow necessary for a reasonable resolution of the (continuous) plane wave with wave length $\lambda = \pi\sqrt{\frac{2}{E}}$. (2.8) can also be written as

$$\alpha_1 = e^{i\bar{k}\Delta x}, \quad \alpha_2 = e^{-i\bar{k}\Delta x},$$

where the *discrete wave vector* $\tilde{k} > 0$ satisfies

$$E = \frac{1 - \cos \tilde{k} \Delta x}{\Delta x^2}.$$

For coarse discretizations, the discrete $E(\tilde{k})$ relation may differ substantially from the analytical $E(k)$ function. Depending on the considered application one hence has to choose between E and k as the fixed input parameter of the problem (2.6). In the sequel we shall consider E as given. For later reference we also assume that $\Delta x < \frac{\pi}{\tilde{k}}$, which is again no practical restriction.

In the right exterior region ($x \geq L$) we have $V = V_L = \text{const}$, and (2.7) again admits solutions of the form

$$\varphi_j = \beta^j, \quad j \geq J, \quad (2.9)$$

with

$$\beta_{1,2} = 1 - (E - V_L) \Delta x^2 \pm i \sqrt{2(E - V_L) \Delta x^2 - (E - V_L)^2 \Delta x^4}. \quad (2.10)$$

Depending on the sign of $E - V_L$ these waves are either traveling or evanescent.

We now turn to the discretization of the two BCs of (2.6). Using one-sided finite differences, a first order discretization reads

$$\begin{aligned} -\gamma_1 \varphi_0 + \varphi_1 &= 2ik \Delta x, \\ \varphi_{J-1} - \gamma_2 \varphi_J &= 0, \end{aligned} \quad (2.11)$$

with $\gamma_1 = 1 - ik \Delta x$ and $\gamma_2 = 1 - i \sqrt{k^2 - 2V_L} \Delta x$. Using centered finite differences one obtains a second order discretization of the BCs. They are also of form (2.11) (after eliminating the ‘ghost points’ φ_{-1} and φ_{J+1} via (2.7)) with $\gamma_1 = 1 - ik \Delta x - \frac{k^2}{2} \Delta x$ and $\gamma_2 = 1 - i \sqrt{k^2 - 2V_L} \Delta x - (\frac{k^2}{2} - V_L) \Delta x^2$. However, both of these discrete BCs would not be satisfied by the above discrete plane waves. And this would introduce spurious oscillations in the numerical solutions as we shall illustrate later. Hence we should rather find the appropriate discretization of the BCs on the discrete level, by considering the discrete plane waves in the vicinity of the two boundaries.

From (2.9) we readily see that the *discrete transparent boundary condition* (DTBC) at $x = L$ reads

$$\varphi_{J-1} - \beta_1^{-1} \varphi_J = 0, \quad (2.12)$$

where the positive sign in (2.10) corresponds to our right traveling waves.

For deriving the DTBC at $x = 0$ we proceed as for the corresponding analytical TBC (2.6): In analogy to (2.5) the solution of the discretized Schrödinger equation (2.7) ‘close’ to the left boundary and in the left exterior region ($j \leq 0$) is a linear combination of the incident and the reflected (discrete) waves:

$$\varphi_j = \alpha_1^j + R \alpha_1^{-j}, \quad j \leq 1. \quad (2.13)$$

Eliminating the discrete reflection coefficient R from φ_0 and φ_1 yields the desired DTBC at $x = 0$:

$$-\alpha_1^{-1} \varphi_0 + \varphi_1 = \alpha_1 - \alpha_1^{-1}. \quad (2.14)$$

We remark that this DTBC cannot be obtained by replacing in (2.11) k by \tilde{k} .

Concerning the solvability of the numerical scheme we have

Theorem 2.1 *Let E , $\{V_j\}$, $j = 0, \dots, J$ be given, and assume $\Delta x < \min\left(\sqrt{\frac{2}{E}}, \frac{\pi}{k}\right)$. Then the discrete BVP (2.7) with either the BCs (2.11) (of first or second order) or the DTBCs (2.14), (2.12) has a unique solution $\{\varphi_j\}$, $j = 0, \dots, J$.*

The simple proof is a discrete analogue of the proof of Proposition 2.3 in [8].

The discrete BCs (2.11) and the DTBCs (2.12), (2.14) are both second order consistent discretizations of the analytical TBCs in (2.6). And one easily verifies that both resulting schemes are convergent for the BVP (2.6). However, the approximation quality is very different for the two discretizations of the BC, as the next example will show.

First we consider the trivial example of (2.6) with $V \equiv 0$ on the interval $x \in (0, 1)$ and we assume that the incoming plane wave has $E = 2000$ and $k = 63.24$. The BVP (2.6) has the simple solution $\varphi(x) = e^{ikx}$, which is plotted in Fig. 1 (real part and absolute value). In the graph this analytical solution coincides with the numerical solution obtained with the DTBCs (2.12), (2.14) on a grid spacing $\Delta x = 1/150$ (implying $\tilde{k} = 63.72$). Using the first and second order discretization (2.11) of the TBCs, however, introduces strong spurious oscillations of $|\varphi(x)|$. We remark that the amplitude of these oscillations would be reduced for finer spatial discretizations. While these oscillations are caused by the inadequate discretization of the TBCs, they propagate all across the interval $(0, 1)$, revealing the wave propagation character of the (stationary) Schrödinger equation (2.6). This situation would be very different for an elliptic two-point BVP.

This simple example already illustrates how important it is to use *discrete transparent boundary conditions* instead of an ad-hoc *discretization of the analytical transparent boundary conditions*.

In the second example we consider an incoming plane wave with energy $E = \frac{k^2}{2} = 656.49$ that hits a potential barrier of height $V_{max} = 656.49$, located in the x -interval $(20, 30)$. The computational interval is $(0, 50)$ with $J = 300$ equidistant grid points. Fig. 2 shows the absolute value of the solution calculated with our DTBCs. Left of the potential barrier one sees the interference pattern of the incoming and the reflected waves.

In this section (as well as in Section 3) we chose a uniform space discretization of the interior problem (i.e. for $0 \leq j \leq J$), *only* to simplify the presentation. The DTBCs at $x = 0$ and $x = L$ are unchanged for a non-uniform discretization inside the interval $(0, L)$.

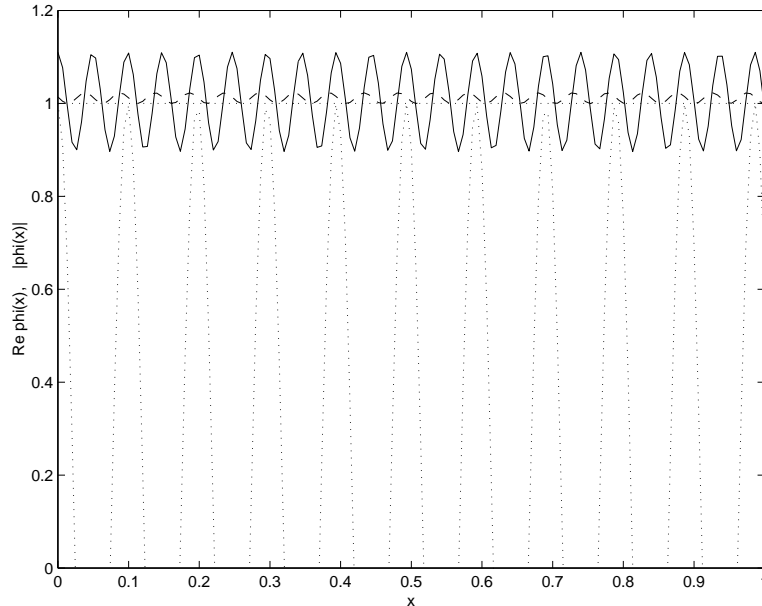


Figure 1: Numerical comparison of the DTBCs and discretized TBCs. Oscillating and straight dotted line: $\text{Re}\varphi(x)$ and $|\varphi(x)|$, respectively; the analytical solution coincides with the numerical solution obtained with DTBCs. Solid and dashed line: absolute value of the numerical solution obtained with discretized TBCs of, resp. first and second order; they both shows spurious oscillations.

3 Transparent BCs for the time-dependent Schrödinger equation

In this section we will carry out the analogous program of §2 for the time-dependent Schrödinger equation. We start again with the 1D whole space problem

$$\begin{aligned} i\hbar\psi_t &= -\frac{\hbar^2}{2m^*}\psi_{xx} + V(x,t)\psi, & x \in \mathbb{R}, t > 0, \\ \psi(x,0) &= \psi^I(x). \end{aligned} \quad (3.1)$$

It models the transient behavior of electrons in a quantum waveguide, e.g., and we assume that the (possibly time-dependent) potential V is given. For $\psi^I \in L^2(\mathbb{R}_x)$ and $V \in C(\mathbb{R}_t^+, L^\infty(\mathbb{R}_x))$ (3.1) has a unique mild solution $\psi \in C(\mathbb{R}_t^+, L^2(\mathbb{R}_x))$ with $\|\psi(\cdot, t)\|_{L^2(\mathbb{R})} = \|\psi^I\|_{L^2(\mathbb{R})}$, $t > 0$ (see [23]).

In order to deal numerically with (3.1) one has to reduce it to a problem on a finite (computational) domain, say $(0, L)$, by introducing artificial BCs outside of the device region (i.e. in the leads of the waveguide). Such BCs, however, should not change the solution of the problem on the interval $(0, L)$. Therefore we shall assume that $\text{supp}(\psi^I) \subset (0, L)$ and that V is constant

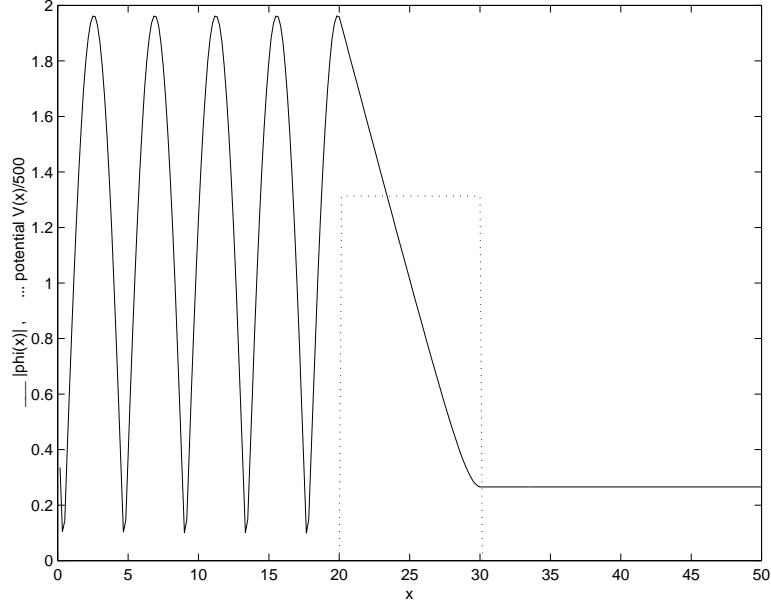


Figure 2: Reflection and transmission of a plane wave at a potential barrier (dotted line). Solid line: absolute value of the numerical solution obtained with DTBCs.

in the leads:

$$\begin{aligned} V(x, t) &= 0, & x \leq 0, t > 0, \\ V(x, t) &= V_L, & x \geq L, t > 0. \end{aligned}$$

Otherwise data of the whole space equation would unavoidably be lost in the reduced problem.

In the 1D case such a *transparent BC* for the transient Schrödinger equation was derived in several different application field, such as quantum mechanics ([6], [16]), optics ([26]), and (underwater) acoustics ([22], [3]).

At the left boundary $x = 0$ the TBC reads

$$\psi_x(0, t) = \sqrt{\frac{2m^*}{\hbar\pi}} e^{-\frac{\pi}{4}i} \frac{d}{dt} \int_0^t \frac{\psi(0, \tau)}{\sqrt{t-\tau}} d\tau, \quad (3.2)$$

where the convolution term can be interpreted as a fractional ($\frac{1}{2}$) time derivative:

$$\frac{1}{\sqrt{\pi}} \frac{d}{dt} \int_0^t \frac{\psi(\tau)}{\sqrt{t-\tau}} d\tau =: \sqrt{\frac{d}{dt}} \psi.$$

Similarly, the right TBC is given by

$$\psi_x(L, t) = -\sqrt{\frac{2m^*}{\hbar\pi}} e^{-\frac{\pi}{4}i} e^{-iV_L t/\hbar} \frac{d}{dt} \int_0^t \frac{\psi(L, \tau) e^{iV_L \tau/\hbar}}{\sqrt{t-\tau}} d\tau. \quad (3.3)$$

These BCs allow the wave packets of the initial wave function to freely leave the computational domain without being reflected at the artificial boundaries. The BCs are non-local in t and of memory-type, thus requiring the storage of all the past history at the boundary in a numerical discretization.

Under some mild regularity assumptions on ψ^I it has been shown that the Schrödinger–BVP (3.1) with the TBCs (3.2) and (3.3) is uniquely solvable, and its solution coincides on the interval $(0, L)$ with the solution of the whole space problem (3.1). As expected, $\|\psi(\cdot, t)\|_{L^2(0,L)}$ decays monotonically in time. For details we refer the reader to [2], [11].

In this paper we shall be mostly interested in inhomogeneous extensions of these TBCs, modeling the continuous influx of a plane wave from the left device contact. The (homogeneous) TBC (3.2) was derived for modeling the situation where an initial wave function is supported in the computational domain $(0, L)$, and it is leaving this domain without being reflected back. If an incoming wave function $\psi^{in}(x, t)$ is given at the left boundary, the inhomogeneous TBC

$$\psi_x(0, t) - \psi_x^{in}(0, t) = \sqrt{\frac{2m^*}{\hbar}} e^{-\frac{\pi}{4}i} \sqrt{\frac{\partial}{\partial t}} [\psi(0, t) - \psi^{in}(t)] \quad (3.4)$$

has to be prescribed at $x = 0$. The right TBC (3.3), however, would be unchanged if no wave enters the computational domain at $x = L$. A typical example for ψ^{in} is a right traveling plane wave

$$\psi^{in}(x, t) = e^{i(kx - \omega t)}, \quad x \leq 0, \quad \omega = \frac{\hbar k^2}{2m^*} = \frac{E}{\hbar}, \quad (3.5)$$

entering the computational domain at the boundary $x = 0$.

Here we shall consider two scenarios where such inhomogeneous TBCs have to be employed. In the first example we model the transition from the vacuum initial state to the steady state with given influx for a quantum structure with time-independent potential $V(x)$. This situation is described by the BVP:

$$\begin{aligned} i\hbar\psi_t &= -\frac{\hbar^2}{2m^*}\psi_{xx} + V(x)\psi, \quad x \in (0, L), \quad t > 0, \\ \psi(x, 0) &= \psi^I(x) := e^{ikx}\chi(x), \quad x \in (0, L), \\ \psi_x(0, t) - \psi_x^{in}(0, t) &= \sqrt{\frac{2m^*}{\hbar}} e^{-\frac{\pi}{4}i} \sqrt{\frac{\partial}{\partial t}} [\psi(0, t) - \psi^{in}(0, t)], \quad t > 0, \\ \psi_x(L, t) &= -\sqrt{\frac{2m^*}{\hbar}} e^{-\frac{\pi}{4}i} e^{-iV_L t/\hbar} \sqrt{\frac{\partial}{\partial t}} [\psi(L, t) e^{iV_L t/\hbar}], \quad t > 0, \end{aligned} \quad (3.6)$$

with ψ^{in} given in (3.5). To avoid a discontinuity at the space-time-corner $(0, 0)$ we assume compatibility of the initial and boundary data at that point. In other words, the incoming wave is assumed to already ‘leak’ a bit into the computational domain at $t = 0$. The monotonously decreasing cut-off function $\chi \in \mathbb{R}$ satisfies $\chi(0) = 1$, $\text{supp}\chi = [0, \varepsilon]$ for some $0 < \varepsilon \ll L$. As we shall illustrate later numerically, the solution of (3.6) converges as $t \rightarrow \infty$ to the unique steady

state $\varphi(x)$ of the BVP (2.6) if the stationary whole space Schrödinger equation (2.1) does not admit bound states. This can be guaranteed by the assumption $V(x) \geq \min(0, V_L)$, e.g.

Our second model concerns the transition behavior of switching between two steady states. We start with a stationary initial condition $\psi^I(x)$ that corresponds to the incoming plane wave $\psi^{in}(x) = e^{ikx}$, $x < 0$ impinging on the potential $V(x)$. In the leads the incoming and reflected plane waves of ψ^I (at $x < 0$) and the transmitted wave (at $x > L$) satisfy (cf. (2.2)-(2.5)):

$$\psi^I(x) = \begin{cases} e^{ikx} + R_k e^{-ikx}, & x < 0, \\ T_k e^{i\sqrt{k^2 - 2m^* V_L/\hbar^2} x}, & x > L. \end{cases} \quad (3.7)$$

Under the whole space Schrödinger equation (3.1) this steady state would evolve as

$$\psi^{st}(x, t) = \psi^I(x) e^{-i\omega t}, \quad (3.8)$$

with $\omega = \frac{\hbar k^2}{2m^*}$. At $t = 0$ we now instantaneously switch the potential to some $W(x)$, which is again constant in the exterior regions $x \leq 0$ and $x \geq L$. For simplicity we assume $V(0) = W(0) = 0$, but V_L and W_L may be different. Due to the switched potential the time evolution of the plane waves (3.7) in the leads changes to

$$\psi^{pw}(x, t) = \begin{cases} \left(e^{ikx} + R_k e^{-ikx} \right) e^{-i\omega t}, & x < 0, \\ T_k e^{i\sqrt{k^2 - 2m^* V_L/\hbar^2} x} e^{-i\omega_L t}, & x > L, \end{cases} \quad (3.9)$$

with $\hbar\omega_L = E + W_L - V_L$. The TBCs (3.2), (3.3) are designed for initial-boundary value problems (IBVPs) with an initial condition supported in $(0, L)$. Hence we have to subtract from the wave function $\psi(x, t)$ the plane waves (3.9) in the leads which then yields inhomogeneous TBCs at both boundaries:

$$\begin{aligned} i\hbar\psi_t &= -\frac{\hbar^2}{2m^*}\psi_{xx} + W(x)\psi, & x \in (0, L), t > 0, \\ \psi(x, 0) &= \psi^I(x), & x \in (0, L), \\ \psi_x(0, t) - \psi_x^{pw}(0, t) &= \sqrt{\frac{2m^*}{\hbar}} e^{-\frac{\pi}{4}i} \sqrt{\frac{\partial}{\partial t}} \left[\psi(0, t) - \psi^{pw}(0, t) \right], & t > 0, \\ \psi_x(L, t) - \psi_x^{pw}(L, t) &= -\sqrt{\frac{2m^*}{\hbar}} e^{-\frac{\pi}{4}i} e^{-iW_L t/\hbar} \sqrt{\frac{\partial}{\partial t}} \left[(\psi(L, t) - \psi^{pw}(L, t)) e^{iW_L t/\hbar} \right], \\ && t > 0. \end{aligned} \quad (3.10)$$

We remark that, in this formulation of the inhomogeneous TBCs, we only need the value and the first x -derivative of the plane wave ψ^{pw} at $x = 0$ and $x = L$.

If $V_L = W_L$ the potential switch could take place at any $t \geq 0$, and the solution of (3.10) will converge as $t \rightarrow \infty$ to the steady state corresponding to $W(x)$ with incoming plane wave $\psi^{in}(x) = e^{ikx}$. If $V_L \neq W_L$, the potential switch has to take place at $t = 0$ since the right exterior potential W_L enters the formulation of the TBCs.

Now we shall turn to the numerical discretization of the TBCs for the time-dependent Schrödinger equation (3.1). For the rest of this section we shall again set $\hbar = m^* = 1$. We consider a Crank–Nicolson finite difference scheme for the Schrödinger equation. With the uniform grid points $x_j = j\Delta x, t_n = n\Delta t$, and the approximations $\psi_j^n \sim \psi(x_j, t_n)$ this scheme reads for the whole space problem

$$\begin{aligned} \frac{i}{\Delta t}(\psi_j^n - \psi_j^{n-1}) &= -\frac{1}{4\Delta x^2}(\psi_{j+1}^n - 2\psi_j^n + \psi_{j-1}^n + \psi_{j+1}^{n-1} - 2\psi_j^{n-1} + \psi_{j-1}^{n-1}) \\ &+ \frac{1}{2}V_j^{n-\frac{1}{2}}(\psi_j^n + \psi_j^{n-1}), \quad j \in \mathbb{Z}, n \in \mathbb{N}, \end{aligned} \quad (3.11)$$

with

$$V_j^{n-\frac{1}{2}} = V(x_j, t_{n-\frac{1}{2}}).$$

For our analysis one of the main advantages of this second order (in Δx and Δt) scheme is its unconditional stability, and it preserves the discrete L^2 -norm:

$$\|\psi^n\|_2^2 = \Delta x \sum_{j \in \mathbb{Z}} |\psi_j^n|^2.$$

As in §2, our main concern is the adequate discretization of the TBCs (3.2), (3.3). In fact, the situation is even more delicate here, as these TBCs involve a convolution with a singular kernel. In [6] and [21] two ‘ad-hoc’ discretizations of the analytical TBC have been proposed. As we shall illustrate below, the resulting schemes introduce spurious numerical reflections at the boundaries and it is only conditionally stable (cf. [21], [2] for details). In [26] a TBC for the (in t) semi-discretized Schrödinger equation was derived which strongly reduces reflections from the boundary.

In [2] the (uniquely determined) *discrete transparent boundary conditions* (DTBC) for the Crank–Nicolson discretization (3.11) of the 1D Schrödinger equation were derived from the fully discrete scheme on the spatial grid $\{x_j\}$, $j \in \mathbb{Z}$. The left (at $j = 0$) and right (at $j = J$) DTBCs are discrete convolutions over the past evolution:

$$\psi_1^n = \sum_{m=1}^n \psi_0^m l_0^{n-m} - \psi_1^{n-1}, \quad \psi_{J-1}^n = \sum_{m=1}^n \psi_J^m l_J^{n-m} - \psi_{J-1}^{n-1}, \quad n \geq 1, \quad (3.12)$$

with

$$\begin{aligned} l_j^n &= \left(1 - i\frac{\rho}{2} + \frac{\sigma_j}{2}\right)\delta_n^0 + \left(1 + i\frac{\rho}{2} + \frac{\sigma_j}{2}\right)\delta_n^1 + \alpha_j e^{-in\varphi_j} \frac{P_n(\mu_j) - P_{n-2}(\mu_j)}{2n-1}, \quad n \geq 0, \\ \rho &= \frac{4\Delta x^2}{\Delta t}, \quad \varphi_j = \arctan \frac{2\rho(\sigma_j + 2)}{\rho^2 - 4\sigma_j - \sigma_j^2}, \quad \mu_j = \frac{\rho^2 + 4\sigma_j + \sigma_j^2}{\sqrt{(\rho^2 + \sigma_j^2)(\rho^2 + [\sigma_j + 4]^2)}}, \\ \sigma_j &= 2\Delta x^2 V_j, \quad \alpha_j = \frac{i}{2} \sqrt{(\rho^2 + \sigma_j^2)(\rho^2 + [\sigma_j + 4]^2)} e^{i\varphi_j/2}, \quad j = 0, J, \end{aligned}$$

where P_n denotes the Legendre polynomials ($P_{-1} \equiv P_{-2} \equiv 0$), and δ_n^j the Kronecker symbol. With our assumptions we have $V_0 = 0$ and $V_J = V_L$.

The P_n only have to be evaluated at the two values μ_0 and μ_J , and hence the numerically stable recursion formula for the Legendre polynomials can be used. Alternatively, the convolution coefficients can be calculated from the simple recursion

$$l_j^n = \frac{2n-3}{n} \mu_j e^{-i\varphi_j} l_j^{n-1} - \frac{n-3}{n} e^{-i2\varphi_j} l_j^{n-2}, \quad n \geq 4.$$

Using asymptotic formulas for the Legendre polynomials one finds $l_0^n, l_J^n = O(n^{-3/2})$ which agrees with the decay of the convolution kernel in the analytical TBCs (3.2), (3.3) (after an integration by parts).

Due to the way our DTBCs are constructed, the Crank–Nicolson scheme (3.11) (for $j = 1, \dots, J-1$) together with the DTBCs (3.12) exactly reproduces the discrete whole space solution of (3.11) (for $j \in \mathbb{Z}$) on the computational grid $x_j, j = 0, \dots, J$. The resulting scheme hence satisfies

$$\|\psi^n\|_2^2 := \Delta x \sum_{j=1}^{J-1} |\psi_j^n|^2 \leq \|\psi^0\|_2^2, \quad n \geq 1, \quad (3.13)$$

and thus it is unconditionally stable.

We remark that the discretizations from [6] and [21] and our DTBCs (3.12) are all consistent discretizations of the analytical TBCs (3.2), (3.3). However, the approximation quality is very different for these two strategies, as the next example will show.

Fig. 3 shows snap shots of the time evolution of the right traveling Gaussian beam ($\psi^I(x) = \exp(100ix - 30(x-0.5)^2)$) evolving under the free Schrödinger equation ($V \equiv 0$) with the rather coarse discretization $\Delta x = 1/160, \Delta t = 0.00002$. Discretizing the analytic TBCs as in Mayfield [21] or as in Baskakov & Popov [6] introduces strong numerical reflections. Our DTBCs (3.12), however, yield the smooth numerical solution to the discrete whole space problem, restricted to the computational interval $[0, 1]$. The Gaussian envelop of the wave packet crosses the right boundary at $x = 1$ without any reflections.

Similar calculations for the transient scattering of wave packets at potential barriers were done in [14]. However, since TBCs were not known then, the authors had to put the problem into a big ‘computational box’, assuming homogeneous Dirichlet BCs at its edges.

Next we shall discuss the discretization of inhomogeneous TBCs. Considering the form of the inhomogeneous TBC of the two models (3.6) and (3.10) we first have to discuss the discretization of the plane waves $\psi^{in}(x, t), \psi^{pw}(x, t)$ and of the static state $\psi^{st}(x, t)$.

The discrete analogue of the right traveling plane wave $\psi^{in}(x, t)$ (cf. (3.5)) with energy E is

$$\phi_j^n = e^{i(\tilde{k}x_j - \tilde{\omega}t_n)}, \quad j \leq 1. \quad (3.14)$$

Since $V_j = 0$ for $j \leq 0$ the plane wave energy and the discrete wave vector \tilde{k} are connected as in §2 by $E = \frac{1 - \cos \tilde{k} \Delta x}{\Delta x^2}$, compared to the analytical analogue $E = \frac{k^2 \hbar^2}{2m^*}$. The discrete plane wave

(3.14) solves the Crank–Nicolson scheme (3.11) for the free Schrödinger equation ($V_j \equiv 0$) in the left exterior domain with the *discrete radian frequency*

$$\tilde{\omega}(E) = \frac{2}{\Delta t} \arctan \frac{\Delta t E}{2}.$$

We remark that the evolution frequency of the corresponding analytical solution of (3.1) would be $\omega = \frac{E}{\hbar}$. We hence have the *discrete dispersion relation*

$$\tilde{\omega}(\tilde{k}) = \frac{2}{\Delta t} \arctan \left[\frac{\Delta t}{2\Delta x^2} (1 - \cos \tilde{k}\Delta x) \right]. \quad (3.15)$$

Next we consider a discrete steady state $\{\varphi_j\}$, $j \in \mathbb{Z}$ solving (2.7) with given E and $\{V_j\}$. Then one easily verifies that

$$\varphi_j e^{-i\tilde{\omega}t_n}, \quad j \in \mathbb{Z}, n \in \mathbb{N}_0, \quad (3.16)$$

solves the whole space Crank–Nicolson scheme (3.11). Assume now that $\{\varphi_j\}$ is a discretization of the initial steady state $\psi^I(x)$ from (3.7), and that it satisfies the discretized stationary Schrödinger equation (2.7) with energy E . (3.16) is then the sought discretization of $\psi^{st}(x, t)$ in (3.8).

Since the (constant) potential in the right lead is switched at $t = 0$ from V_L to W_L , one has to adapt the evolution frequency of the transmitted plane wave. Following our discussions above, the adequate discretization of $\psi^{pw}(x, t)$ in (3.9) reads:

$$\phi_j^n = \begin{cases} \varphi_j e^{-i\tilde{\omega}t_n}, & j \leq 1, n \in \mathbb{N}_0, \\ \varphi_j e^{-i\tilde{\omega}_L t_n}, & j \geq J-1, n \in \mathbb{N}_0, \end{cases} \quad (3.17)$$

with

$$\tilde{\omega}_L(E) = \frac{2}{\Delta t} \arctan \frac{\Delta t(E + W_L - V_L)}{2}.$$

Now we can formulate the discretization of the inhomogeneous TBC from (3.6) and (3.10), resp. The DTBCs are obtained by simply replacing ψ_j^n in (3.12) by $\psi_j^n - \phi_j^n$, where ϕ_j^n is given for the first example by (3.14) and $\phi_j^n = \phi_{j-1}^n = 0$, and for the second model by (3.17):

$$\begin{aligned} \psi_1^n - \phi_1^n &= \sum_{m=1}^n (\psi_0^m - \phi_0^m) l_0^{n-m} - (\psi_1^{n-1} - \phi_1^{n-1}), \quad n \geq 1, \\ \psi_{J-1}^n - \phi_{J-1}^n &= \sum_{m=1}^n (\psi_J^m - \phi_J^m) l_J^{n-m} - (\psi_{J-1}^{n-1} - \phi_{J-1}^{n-1}), \quad n \geq 1. \end{aligned} \quad (3.18)$$

The convolution coefficients l_j^n for the right DTBC are given in (3.12), where the potential V_j equals either V_L or W_L in our two examples.

We shall now present simulations for the two models (3.6) and (3.10) to illustrate how these DTBCs work. For both calculations we consider a quantum waveguide of length $L = 50\text{nm}$

with a 10nm thick rectangular potential barrier of height $V_{max} = 0.3\text{eV}$ (corresponding to an $\text{Al}_x\text{Ga}_{1-x}\text{As}$ barrier within GaAs bulk material). The effective mass of the electrons is $m^* = 0.0667m_0$ (corresponding to GaAs) and it is assumed constant in the device region. We use the discretization $\Delta x = 0.167\text{nm}$ and $\Delta t = 0.288\text{fs}$.

EXAMPLE 1: As described by (3.6), a right traveling plane wave with $k = 0.7247(\text{nm})^{-1}$ (and $\tilde{k} = 0.7251$) is scattered at the potential barrier. The wave energy is $E = \frac{k^2\hbar^2}{2m^*} = 0.3\text{eV}$. At $t = 0$ the incoming plane wave reaches until $x = 16.7\text{nm}$, and we have chosen a piecewise cubic cut-off $\chi(x)$ (cf. (3.6)). Fig. 4 shows snap shots of this temporal evolution. At $t = 14\text{fs}$ one sees the starting interference of the incoming and the reflected plane waves. At $t = 202\text{fs}$ a steady state has already been reached, and it coincides with the steady state calculated with the stationary Schrödinger equation (see. Fig. 2). We remark that the shown numerical solutions coincide exactly with the numerical solution on the spatial grid $x_j = j\Delta x$, $j \in \mathbb{Z}$, as intended by DTBCs.

Fig. 4 also shows the temporal behavior of the electric current through the device (averaged in $x \in (0, L)$)

$$J(x, t) = \frac{\hbar e_0}{2m^*} \text{Im}(\psi \bar{\psi}_x).$$

It indicates that a steady state is reached after about 0.2ps.

EXAMPLE 2: Here we consider the switching behavior of the quantum structure when applying a linear bias of -0.1eV across the device subinterval $[10\text{nm}, 40\text{nm}]$. Using Wigner function models similar situations were studied in [27] for a single potential barrier and in [12], [15] for a double potential structure.

Here we solve the system (3.10) with our inhomogeneous DTBC (3.17), (3.18). The initial condition ψ^I is the steady state from Example 1, and at $t = 0$ the bias is switched on instantaneously, yielding the potential $W(x)$. Fig. 5 shows snap shots of the evolution of the wave function. The time behavior of the current indicates that the new steady state is reached after about 0.2ps.

The plot of the current also shows the temporal behavior of the current for the reverse switching. When switching off the applied bias at $t = 0$ the current first overshoots and reaches a stationary level again after about 0.2ps.

4 Boundary conditions for the Wigner equation

In this section we review several options for prescribing BCs for the Wigner equation in 1D:

$$\begin{aligned} w_t + vw_x - \frac{1}{m^*} \Theta[V]w &= 0, & x \in (0, L), v \in \mathbb{R}, t > 0, \\ w(x, v, 0) &= w^I(x, v), & x \in (0, L), v \in \mathbb{R}, \end{aligned} \quad (4.1)$$

with the pseudo-differential operator (1.3) and the initial Wigner function $w^I(x, v)$.

Due to its kinetic structure we have to prescribe BCs for the Wigner function $w(x, v, t)$ at those boundary parts of the phase space slab that correspond to incoming velocities: $(x = 0, v)$, $v > 0$ and $(x = L, v)$, $v < 0$. The simplest strategy is to use *inflow boundary conditions*, where one specifies the distribution flowing into the device region through the boundary (either in the stationary or the time-dependent case):

$$\begin{aligned} w(0, v, t) &= f^+(v, t), & v > 0, t > 0, \\ w(L, v, t) &= f^-(v, t), & v < 0, t > 0. \end{aligned} \quad (4.2)$$

Typically, $f^\pm(v, t)$ are the thermal equilibrium distribution functions (Fermi–Dirac) of the electron reservoir, which is coupled to the device at the contacts. Although rather simple, such BCs were successfully employed in the Wigner simulations of resonant tunneling structures ([12], [13]) and quantum waveguides ([27]). We remark that these BCs are not completely satisfactory from the modeling point of view, as they usually cannot guarantee that the resulting Wigner function will correspond to a positive density matrix operator (cf. [4], [20]). However, this does not pose a serious problem in simulations, if such (classically inspired) inflow BCs are not placed too close to heterojunctions or discontinuities of the potential V , as those are the dominant ‘sources’ of quantum effects.

Mathematically, the transient and stationary Wigner equation with inflow BCs was analyzed, respectively, in [19] and in [4]. Using semigroup techniques it was found that the transient IBVP is well-posed in $C([0, \infty), L^2((0, L) \times \mathbb{R}))$ under very mild assumptions on the boundary data and the potential.

The stationary situation, however, is much more delicate: in [4] the authors considered a velocity semi-discretization (with velocity grid points $\{v_j\}$, $j \in \mathbb{Z}$) of the stationary Wigner equation

$$vw_x - \frac{1}{m^*} \Theta[V]w = 0, \quad x \in (0, L), v \in \mathbb{R}. \quad (4.3)$$

The resulting ODE-BVP is well-posed only if zero is not chosen as a discrete velocity ($0 \notin \{v_j\}$). In the continuous velocity situation the stationary Wigner BVP (4.3), (4.2) is well posed under some technical assumptions on the boundary data ([5]). This contrasts the classical counterpart situation - the stationary BVP for the Liouville equation, which may have closed trajectory loops ([7]). Consequently, the classical solution is not determined by the boundary data on such closed trajectories.

In [24], [1] a hierarchy of *absorbing boundary conditions* (ABCs) have been devised for the transient Wigner equation as a refinement of inflow BCs. They account for the coupling of the incoming and outgoing distribution at the boundary in quantum kinetic models. These ABCs are non-local in time and the lowest order ABC reads:

$$\begin{aligned} w^+(0, v, t) &= f^+(v, t) + \int_0^t (M_1 w^-)(0, v, \tau) d\tau, & v > 0, t > 0, \\ w^-(L, v, t) &= f^-(v, t) + \int_0^t (M_1 w^+)(L, v, \tau) d\tau, & v < 0, t > 0, \end{aligned} \quad (4.4)$$

where we have used the notation

$$w^\pm(v) = w(v)H(\pm v), \quad v \in \mathbb{R},$$

with the Heaviside function $H(v)$. In Equation (4.4) f^\pm denote the prescribed inflow into the domain $(0, L)$, like in (4.2). The pseudo-differential operator M_1 is defined as

$$(M_1 w^-)(0, v, t) = \frac{i}{\sqrt{2\pi m^*}} \int_{-\infty}^0 (\mathcal{F}_\eta \partial V)(x=0, v' - v, t) \frac{v'}{v' - v} w^-(0, v', t) dv', \quad v > 0,$$

$$(M_1 w^+)(L, v, t) = \frac{i}{\sqrt{2\pi m^*}} \int_0^\infty (\mathcal{F}_\eta \partial V)(x=L, v' - v, t) \frac{v'}{v' - v} w^+(L, v', t) dv', \quad v < 0,$$

with \mathcal{F}_η denoting the Fourier transform w.r.t. the variable η .

Using semigroup techniques it was shown in [1] that the IBVP (4.1), (4.4) has a unique solution $w \in C([0, \infty), L^2((0, L) \times \mathbb{R}))$ for initial data $w^I \in L^2((0, L) \times \mathbb{R})$ and inflow data $f^\pm \in L^2_{loc}((0, \infty), L^2(\mathbb{R}^\pm, |v|))$. The main ingredient for this result is the boundedness of the boundary operator M_1 from $L^2(\mathbb{R}^\mp, |v|)$ into $L^2(\mathbb{R}^\pm, |v|)$. This boundedness holds if $V, \mathcal{F}_x V \in L^1(\mathbb{R}_x)$, e.g.

Acknowledgement

The author was partially supported by the grants ERBFMRXCT970157 (TMR-Network) from the EU and the DFG under Grant-No. MA 1662/1-3.

References

- [1] A. Arnold, *On Absorbing Boundary Conditions for Quantum Transport Equations*, Math. Modell. Num. Anal. **28**, 7, 853–872, 1994.
- [2] A. Arnold, *Numerically absorbing boundary conditions for quantum evolution equations*, VSLI Design, **6**, 1–4, 313–319, 1998.
- [3] A. Arnold, M. Ehrhardt, *Discrete transparent boundary conditions for wide angle parabolic equations in underwater acoustics*, J. Comput. Physics **145**, 2, 611–638, 1998.
- [4] A. Arnold, H. Lange, P.F. Zweifel, *A discrete-velocity, stationary Wigner equation*, submitted to J. Math. Phys., 1999.
- [5] A. Arnold, H. Lange, *Well-posedness of the stationary Wigner equation with inflow boundary conditions*, in preparation, 1999.

- [6] V.A. Baskakov, A.V. Popov, *Implementation of transparent boundaries for numerical solution of the Schrödinger equation*, Wave Motion **14**, 123–128, 1991.
- [7] N. Ben Abdallah, *A Hybrid Kinetic-Quantum Model for Stationary Electron Transport in a Resonant Tunneling Diode*, J. Stat. Phys. **90**, 3-4, 627–662, 1998.
- [8] N. Ben Abdallah, P. Degond, P.A. Markowich, *On a One-Dimensional Schrödinger-Poisson Scattering Model*, ZAMP **48**, 1, 135–155, 1997.
- [9] L. Burgnies, *Mécanismes de conduction en régime balistique dans les dispositifs électroniques quantiques*, Ph.D.-thesis at l'Université des Sciences et Technologies de Lille, France, 1997.
- [10] P. Butcher, N.H. March, M.P. Tosi, *Physics of Low-Dimensional Semiconductor Structures*, Plenum Press, New York - London, 1993.
- [11] L. Di Menza, *Approximations numériques d'équations de Schrödinger non linéaires et de modèles associés*, PhD thesis, Université Bordeaux I, 1995.
- [12] W.R. Frensley, *Wigner function model of a resonant-tunneling semiconductor device*, Phys. Rev. B. **36**, 1570–1580, 1987.
- [13] W.R. Frensley, *Boundary conditions for open quantum systems driven far from equilibrium*, Rev. Modern Phys. **62**, 3, 745–791, 1990.
- [14] A. Goldberg, H.M. Schey, J.L. Schwartz, *Computer-Generated Motion Pictures of One-Dimensional Quantum-Mechanical Transmission and Reflection Phenomena*, Amer. J. Phys. **35**, 177–186, 1967.
- [15] K.K. Gullapalli, D.R. Miller, D.P. Neikirk, *Simulation of quantum transport in memory-switching double-barrier quantum-well diodes*, Phys. Rev. B. **49**, 2622–2628, 1994.
- [16] J.R. Hellums, W.R. Frensley, *Non-Markovian open-system boundary conditions for the time-dependent Schrödinger equation*, Phys. Rev. B **49**, 2904–2906, 1994.
- [17] N. Kluksdahl, A.M. Kriman, D.K. Ferry, C. Ringhofer, *Self-Consistent Study of the Resonant Tunneling Diode*, Phys. Rev. B. **39**, 7720–7735, 1989.
- [18] C.S. Lent, D.J. Kirkner, *The quantum transmitting boundary method*, J. Appl. Phys., **67**, 6353–6359, 1990.
- [19] P.A. Markowich, C. Ringhofer, *An Analysis of the Quantum Liouville Equation*, ZAMM **69**, 121–127, 1989.
- [20] P.A. Markowich, C. Ringhofer, C. Schmeiser, *Semiconductor Equations*, Springer, New York, 1990.

- [21] B. Mayfield, *Non-local boundary conditions for the Schrödinger equation*, Ph.D. thesis, University of Rhode Island, Providence, RI, 1989.
- [22] J.S. Papadakis, *Impedance formulation of the bottom boundary condition for the parabolic equation model in underwater acoustics*, NORDA Parabolic Equation Workshop, NORDA Tech. Note 143, 1982.
- [23] A. Pazy, *Semigroups of Linear Operators and Applications to Partial Differential Equations*, 2nd Edition, Springer, 1992.
- [24] C. Ringhofer, D. Ferry, N. Kluksdahl, *Absorbing Boundary Conditions for the Simulation of Quantum Transport Phenomena*, Trans. Theo. Stat. Phys., **18**, 331-346, 1989.
- [25] C. Ringhofer, *Computational Methods for Semiclassical and Quantum Transport in Semiconductor Devices*, Acta Numerica, **3**, 485–521, 1997.
- [26] F. Schmidt, P. Deuffhard, *Discrete transparent boundary conditions for the numerical solution of Fresnel's equation*, Computers Math. Applic. **29**, 53–76, 1995.
- [27] H. Tsuchiya, M. Ogawa, T. Miyoshi, *Wigner Function Formulation of Quantum Transport in Electron Waveguides and Its Application*, Jap. J. Appl. Phys., **30**, 3853–3858, 1991.

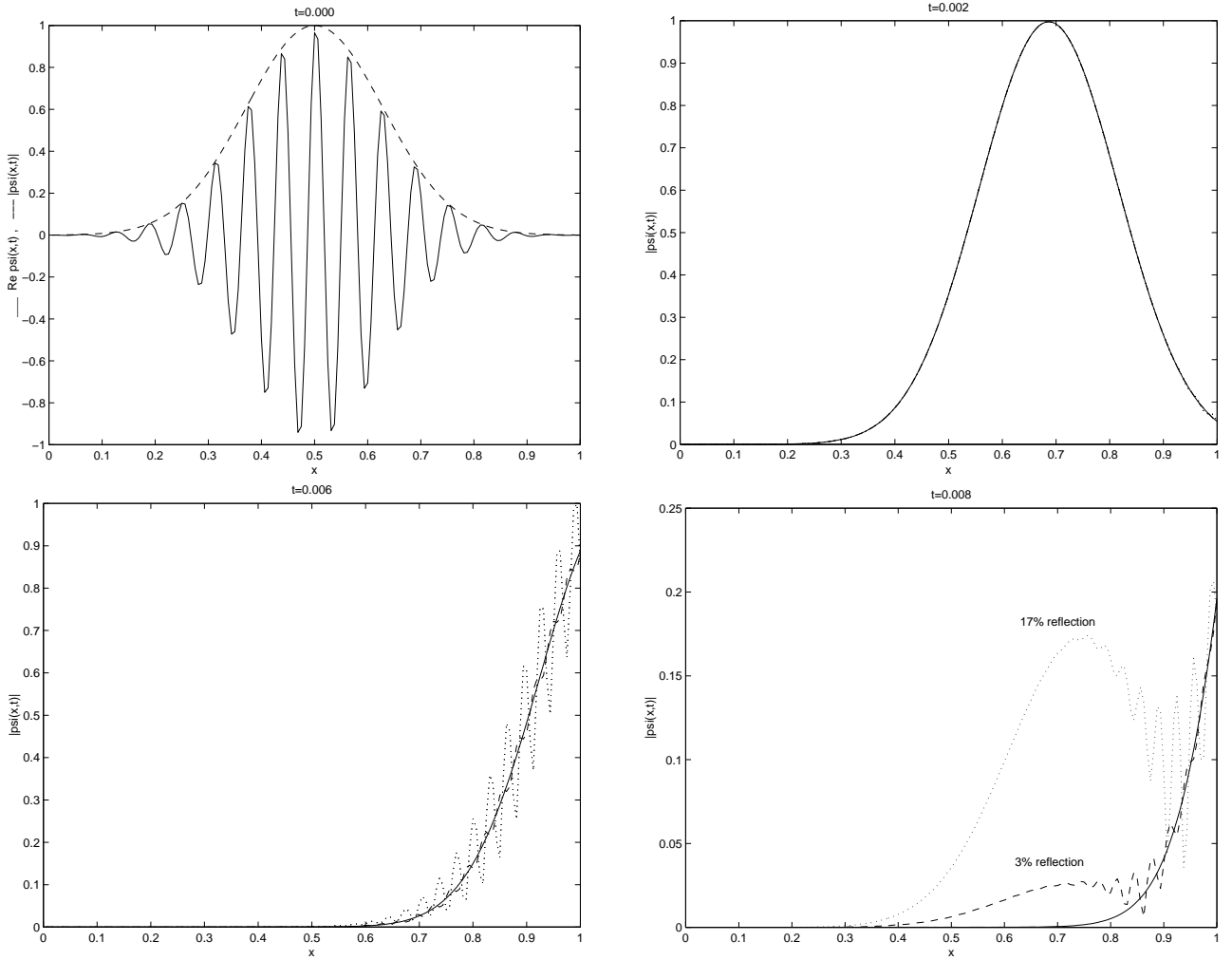


Figure 3: Gaussian wave packet, traveling to the right. Top left figure: $\text{Re } \psi^I(x)$ (solid line), $|\psi^I(x)|$ (dashed line). Remaining figures: numerical comparison of $|\psi(x, t)|$ calculated with DTBCs and discretized TBCs at $t = 0.002$, $t = 0.006$, and $t = 0.008$. Solid line: The numerical solution obtained with our DTBCs coincides with the exact analytical solution. The solution obtained with the discretized TBCs of Mayfield (dotted line) and Baskakov & Popov (dashed line) shows strong numerical reflections from the right boundary.

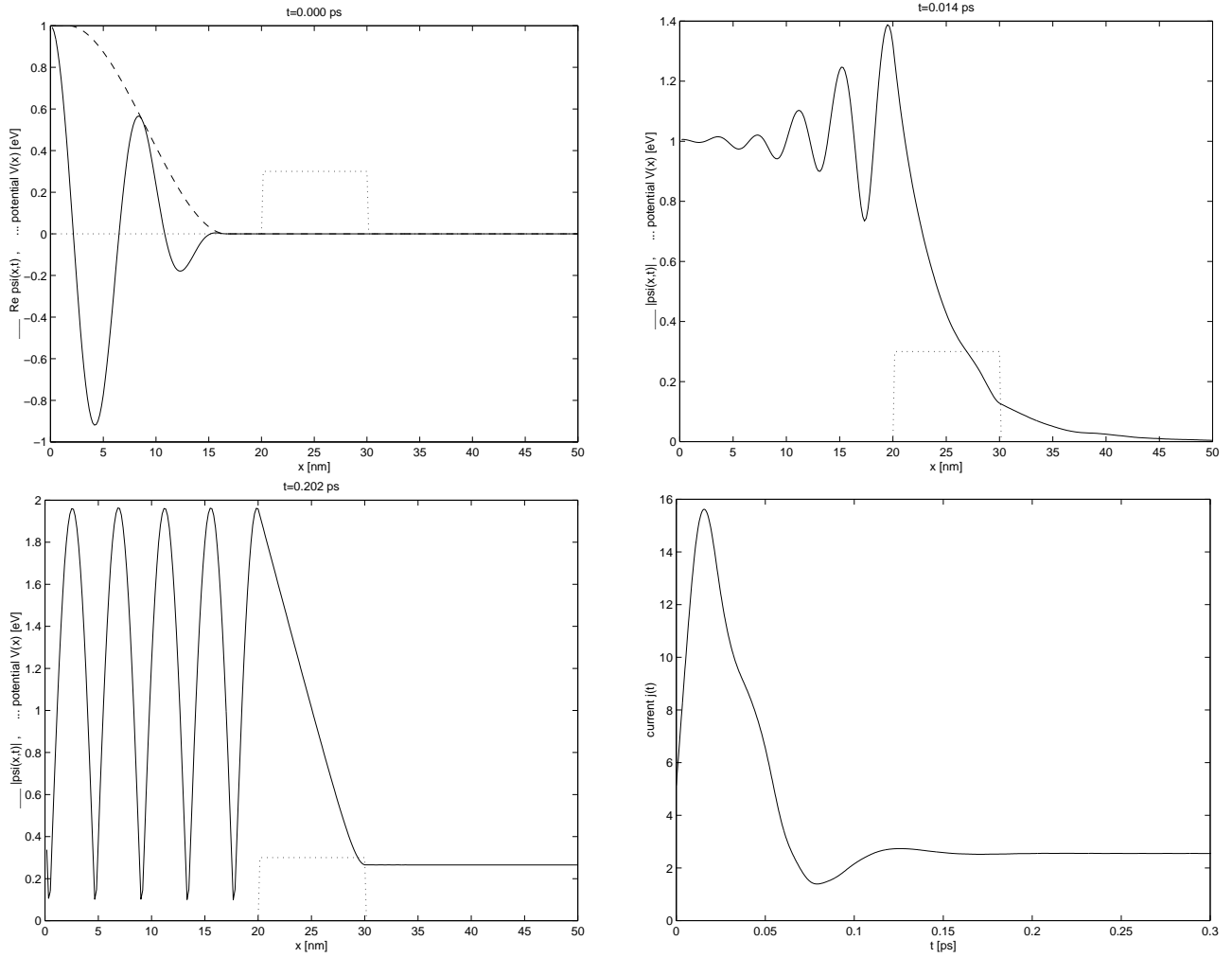


Figure 4: Right traveling plane wave scattered at a potential barrier (dotted line). Top left figure: $\text{Re } \psi^I(x)$ (solid line) and $|\psi^I(x)|$ (dashed line). Top right and bottom left figure: wave function $|\psi(x, t)|$ calculated with inhomogeneous DTBCs at $t = 0.014$ ps and $t = 0.202$ ps (solid line). Bottom right figure: time evolution of the average current $j(t)$.

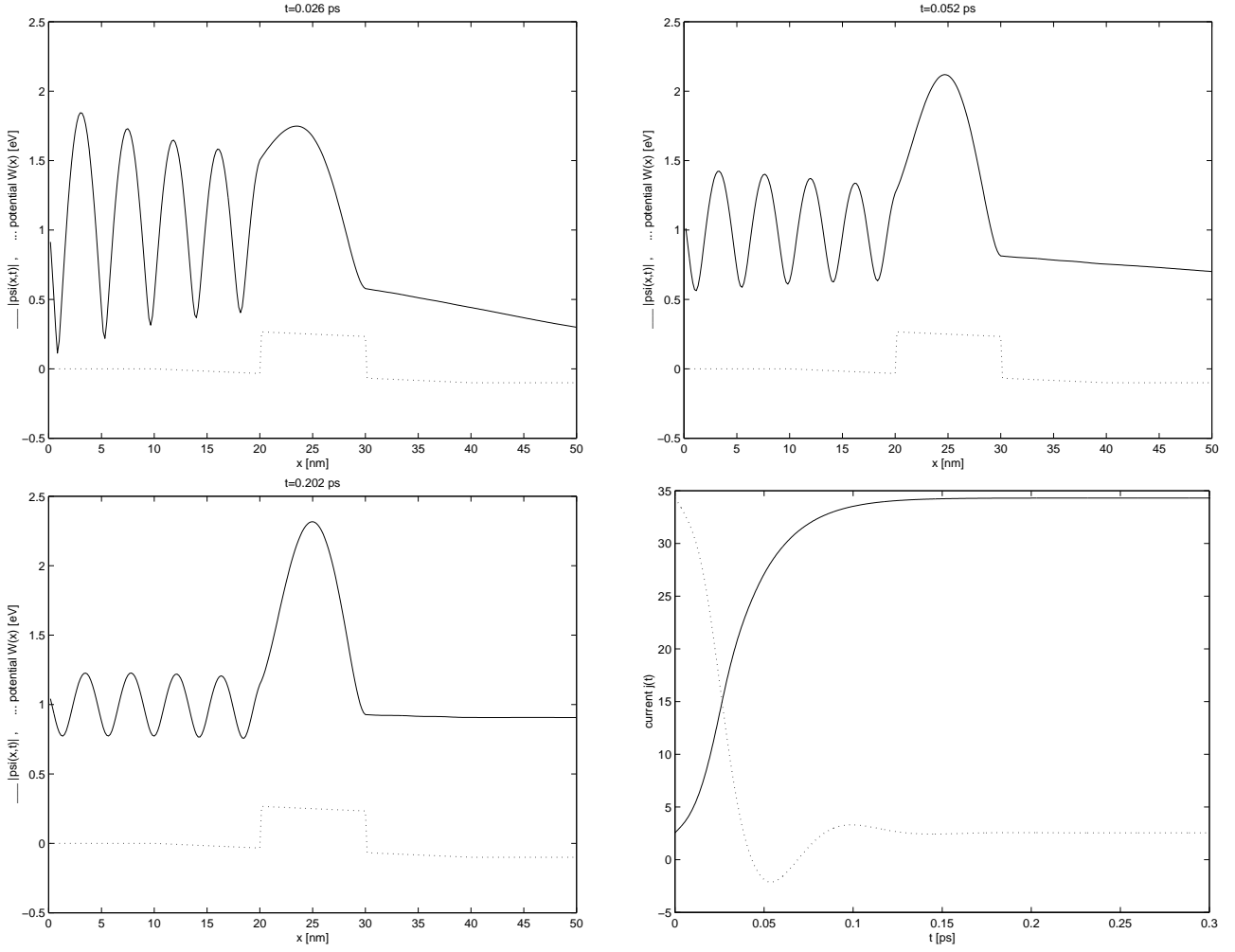


Figure 5: Switching the applied bias. Bottom right figure: time evolution of the average current $j(t)$ when switching from 0 eV to -0.1 eV (solid line) and from -0.1 eV to 0 eV (dotted line). Remaining figures: evolution of the wave function $|\psi(x, t)|$ calculated with inhomogeneous DTBCs at $t = 0.026$ ps, $t = 0.052$ ps, and $t = 0.202$ ps (solid line) as a response to switching the potential from $V(x)$ to $W(x)$ (dotted line) at $t = 0$.